Transient optogenetic inactivation of the medial entorhinal cortex biases the active population of hippocampal neurons

J.W. Rueckemann[1], **A.J. DiMauro**[1], **L.M. Rangel**[1], **X. Han**[2], **E.S. Boyden**[3], and **H. Eichenbaum**[1]

[1]Center for Memory and Brain, Boston University, Boston, MA 02215

[2]Biomedical Engineering, Boston University, Boston, MA 02215

[3]Biological Engineering, Massachusetts Institute of Technology, Cambridge, MA 02139

Abstract

The mechanisms that enable the hippocampal network to express the appropriate spatial representation for a particular circumstance are not well understood. Previous studies suggest that the medial entorhinal cortex (MEC) may have a role in reproducibly selecting the hippocampal representation of an environment. To examine how ongoing MEC activity is continually integrated by the hippocampus, we performed transient unilateral optogenetic inactivations of the MEC while simultaneously recording place cell activity in CA1. Inactivation of the MEC caused a partial remapping in the CA1 population, without diminishing the degree of spatial tuning across the active cell assembly. These changes remained stable irrespective of intermittent disruption of MEC input, indicating that while MEC input is integrated over long time scales to bias the active population, there are mechanisms for stabilizing the population of active neurons independent of the MEC. We find that MEC inputs to the hippocampus shape its ongoing activity by biasing the participation of the neurons in the active network, thereby influencing how the hippocampus selectively represents information.

Keywords

hippocampus; CA1; place cell; ArchT; inactivation

Introduction

To selectively utilize memory based on meaningful circumstances, there must be a mechanism for activating particular representations in the hippocampus. Distinct activity profiles across the population of its spatially selective neurons, termed *place cells*, allow the hippocampus to form different maps of each spatial environment (Alme et al., 2014; Muller and Kubie, 1987; O'Keefe and Dostrovsky, 1971; O'Keefe and Nadel, 1978). The active hippocampal ensemble is also readily reorganized in response to changing task conditions (Dupret et al., 2010; Markus et al., 1995; Moita et al., 2004), allowing the hippocampus to

Corresponding author: Howard Eichenbaum, 2 Cummington Mall, Boston, MA 02215, 617-353-1426, hbe@bu.edu.

flexibly represent an environment based on salient events. This capacity to selectively activate hippocampal spatial representations may be an example of a more general ability to recollect specific experiences from memory (Eichenbaum et al., 2012).

The mechanisms that allow the hippocampal network to express a particular spatial representation are not well understood. It is possible that the spatial firing patterns of hippocampal neurons are directly inherited from afferent structures, particularly the medial entorhinal cortex (MEC), which also exhibits a high degree of spatially selective activity (Bjerknes et al., 2014; Fyhn et al., 2004; Giocomo et al., 2014; Hafting et al., 2005; Sargolini et al., 2006). This view is supported by multiple theoretical models that posit that the MEC is the driver of spatial specificity in the hippocampus (Fyhn et al., 2007; McNaughton et al., 2006; Rolls et al., 2006; Savelli and Knierim, 2010). However, several lesion and inactivation studies have complicated this portrayal. They find that the reproducibility of place fields across exposures to the same environment depends on MEC input, but the existence of place fields does not (Brandon et al., 2014; Van Cauter et al., 2008; Hales et al., 2014; Miller and Best, 1980; Navawongse and Eichenbaum, 2013; Schlesiger et al., 2015). This dissociation of function suggests that there are separable mechanisms that give rise to hippocampal spatial representations, and that the MEC may be particularly important for activating the appropriate representation.

Although previous intervention studies broadly characterize the MEC as necessary for the reproducible mapping of an environment during long timescales, it is not known if the MEC influences the hippocampus on the order of seconds as the animal experiences an environment. As a result, it remains unclear whether activity from the MEC is continually integrated into the hippocampal network within the same experience. If CA1 is perpetually dependent on MEC input to activate the appropriate spatial representation of an environment, then temporally acute manipulations of MEC would result in synchronized changes in the population of active CA1 neurons. Alternatively, CA1 may receive a bias from extrinsic inputs towards activating particular cell assemblies, and utilizes additional mechanisms to drive cell activity and stabilize the population of active neurons. Under this hypothesis, CA1 activity would not exhibit time-locked changes to intermittent MEC disruption. By using a short duration inactivation, it is possible to directly test these hypotheses and observe how the removal of input affects the hippocampal representation as the animal is processing an environment.

We used the optogenetic inhibitory opsin, archaerhodopsin (ArchT) (Boyden, 2011; Han et al., 2011), to periodically disrupt activity on the timescale of seconds within the dorsocaudal MEC while recording the spatial firing of dorsal CA1 hippocampal neurons. By transiently disrupting a restricted set of afferents to the hippocampus, we also investigated whether altering a small set of inputs is sufficient to create a wholly orthogonal spatial representation. We found that unilateral inactivations of the MEC resulted in a partial remapping across the population and that after cells remapped they remained stable irrespective of subsequent intermittent disruption of MEC input. This remapping did not result in a net change in spatial information across the population, and the number of place fields that were lost was balanced by the place fields that were gained. Transient disruption of the MEC thus enabled the activation of a different hippocampal spatial map, without

diminishing the degree of spatial tuning of the population. Our results elucidate how the inputs to the hippocampus continually shape its ongoing activity, revealing mechanisms that influence the selective recruitment of neural representations.

Materials and Methods

Subjects

The subjects for these experiments were seven male Long-Evans rats (Charles River Laboratories) weighing 350–400g at the start of the experiment (4 ArchT and 3 GFP; see below). Rats were housed individually and maintained on a 12-hour light/dark cycle in the Laboratory Animal Care Facility at Boston University. Upon arrival animals were habituated to the facility for a minimum of one week and were then handled by experimenters 20 minutes per day for one week prior to behavioral training. Animals were food restricted to maintain a weight at least 85% of free-feeding weight and had access to water *ad libitum*. Behavioral training was done during the light phase of the cycle. All procedures were performed with the approval of the Boston University Institutional Animal Care and Use Committee and accordance with all national and local guidelines.

Implant Construction and Surgery

Each rat was implanted with a microdrive containing 12–20 independently movable tetrodes directed toward CA1 and an optic fiber in the dorsocaudal MEC. Each tetrode comprised four 12μm nichrome wires (Sandvik Heating Technology), and was gold-plated until an impedance of 200–250 kΩ at 1000 Hz was reached (Komorowski et al., 2009). The optic fiber consisted of a 200 μm fiber (30 μm cladding, 250 μm jacketing, 0.39 numerical aperture) terminating in a SMA connector (ThorLabs). The implanted end of the fiber (6mm) was stripped of outer jacketing to reduce the diameter and minimize tissue damage. A scored 25-gauge cannula was glued above the stripped segment, creating a rough surface that improved the adherence of the implantation acrylic. Before implantation, a light intensity curve was constructed for each fiber to ensure an irradiance of 100–200 mW/mm^2 at the tip of the fiber. The optic fiber was implanted separately from the microdrive, and was integrated into the microdrive during the surgery. The outside of the optic fiber implant was coated in black acrylic paint after surgery to ensure that light from the optic fiber was not visible by the animal.

Surgery

All surgeries were performed stereotactically. The viral infusion was delivered through a 30-gauge cannula lowered into the right dorsocaudal MEC (AP: –9.5, ML: - 5.2, DV: –4.3) at a rate of 50 nl/min from a 10μl Hamilton syringe to total volume of 1μl. The cannula was left in place for 10 minutes following infusion to allow viral diffusion away from the tip. After retraction of the cannula, a fiber optic cable was lowered into the site of the viral infusion and secured in place (Figure 1A,B). The microdrive was implanted over the right dorsal CA1 (AP: –3.6, ML: – 2.8), and the SMA connector of the fiber optic was affixed to the microdrive using dental acrylic (Figure 1A). Rat health was monitored during a post-surgical recovery period that lasted at least one week.

Optogenetic Virus and Light Delivery

Optogenetic inactivation was achieved using the light sensitive outward-directed proton pump ArchaerhodopsinT (ArchT), which hyperpolarizes neurons upon exposure to yellow-green light (Han et al. 2011). An adeno-associated viral vector (serotype 8) with the hybrid cytomegalovirus (CMV) enhancer/chicken beta actin (CAG) pan-neuronal promoter was used to infect neurons. Protein expression was not specific to neuron type, and expression was present in all layers of MEC surrounding the injection site (Figure 1C). Four rats received virus coding the protein ArchT (AAV8-CAG-ArchT-GFP; University of North Carolina vector core). These rats composed the experimental ArchT rat group. Three additional rats received virus that did not code for ArchT but was otherwise identical (AAV8-CAG-GFP; University of North Carolina vector core). These rats composed the GFP rat group, which provided a control for non-specific effects of light stimulation. Virus injected at a titer of 10^{12} viral particles/ml.

Light was delivered via a chronically implanted 200 μm fiber coupled to an SMA connector. During recording days a 200 μm patch cable connected the optic fiber implant to a 532-nm laser (Shanghai Laser & Optics Century Co., Ltd). Laser illumination was controlled via TTL pulses delivered by a digital input/output box (NI-6501, National Instruments) under the control of custom software (MATLAB). The timing of the analog laser control signal was monitored by an Omniplex recording system and synchronized with neural data and video tracking.

Electrophysiological Recordings

To allow time for optimal expression of ArchT, tetrodes were advanced to the dorsal CA1 region over a minimum period of four weeks. The positions of tetrodes were estimated using turn counts (282 μm per turn) and electrophysiological features characteristic of CA1 including the presence of theta oscillations, sharp-wave ripple events and theta-modulated complex spiking activity. Signals were amplified 4000–8000 times, bandpass filtered between 400 Hz and 8000 Hz to capture spike activity and digitized at 40 kHz by an Omniplex Neural Acquisition system (Plexon, Inc.). Position data was captured using LEDs situated on the rat's head stage that were monitored at 30 Hz by a Cineplex Digital Capture System (Plexon, Inc.) and synchronized to neural data.

Behavioral Paradigm and Inactivation Schedule

Prior to implantation, rats were trained to run in one direction around an elliptical track with a circumference of 346 cm (Figure 1D). Rats were rewarded with ¼ size Froot Loop® pieces at a consistent location upon the completion of each lap. The width of the track was 5 cm to discourage turning. Behavioral training was complete when the rat could consistently finish 45 minutes of self-initiated, unidirectional running.

Two groups of rats were tested in this experiment: rats that expressed ArchT in the MEC (ArchT group) and control rats that expressed GFP but not ArchT (GFP group). On experimental days, every rat either received laser stimulation to inactivate the MEC (Laser) (Figure 1E, top) or a sham-laser treatment in which the laser was prevented from shining through the fiber optic (Sham-Laser) (Figure 1E, bottom). Sham-Laser intervention days

provided a within-animal comparison to Laser intervention days. Each recording day started with a baseline period (Baseline) that lasted approximately 10 minutes, during which the rat ran around the track without any intervention. This Baseline period provided an opportunity to characterize the spatial tuning of the hippocampal neurons at the start of the recording. The Baseline was followed by a 25-minute intervention period (Intervention), which comprised intervals with the laser on (Laser-On) and the laser turned off (Laser-Off). Laser-On intervals lasted 10 seconds and were followed by variable Laser-Off delays (17.5 to 22.5 seconds), which are represented in Figure 1E (top) by green lines and gray spaces, respectively. Intervals that were temporally matched to the Laser-On and Laser-Off intervals were delineated during the Sham-Laser days (Figure 1E, bottom), though no light was delivered to the rat during Sham Laser-On intervals. Since the Laser-On intervals were initiated according to a temporal schedule, the position of the animal was effectively random for every Laser-On interval. There were 30 Laser-On intervals per day for a total of 300 seconds over the intervention period. After the rat was returned to the home cage for 1–2 hours, a 35-minute recovery period (Recovery) was recorded as the rat ran around the maze without any laser intervention. The recovery period permitted the characterization of the hippocampal network after the inactivation.

Across the 4 ArchT rats, there were a total of 28 Laser intervention days (ArchT1 = 7, ArchT2 = 7, ArchT3 = 6, ArchT4 = 8), and a total of 20 Sham-Laser intervention days (ArchT1 = 6, ArchT2 = 6, ArchT3 = 6, ArchT4 = 2). Across the 3 GFP rats, there were a total of 22 Laser intervention days (GFP1 = 7, GFP2 = 9, GFP3 = 6), and a total of 16 Sham-Laser intervention days (GFP1 = 6, GFP2 = 6, ArchT3 = 4).

Unit Identification

Individual units were isolated by manually sorting clusters of waveforms using Offline Sorter (Plexon, Inc.). Sorting was performed using the relative amplitudes across each wire, the waveform width, and the peak to valley distance. The sorted clusters were screened for inter-spike intervals shorter than the neuronal refractory period, indicating that there could be multiple units. Spiking and tracking data were imported into MATLAB for further analysis with custom scripts.

Spatial Rate Maps

Spatial firing rate maps were made for each unit to show the location specific activity. The environment was parsed into 2.5×2.5 cm bins, and for each bin the firing rate was calculated as the total number of spikes divided by the total amount of time the animal spent in that bin. To be included in the analyses the bin must have been occupied for a minimum of 300 ms. Intervals when the animal was moving less than 7 cm/s were excluded from analysis. Each unit categorized as a place cell had a mean firing rate less than 5 Hz, an in-field firing rate greater than 1 Hz, and at least seven adjacent pixels with a firing rate greater than two standard deviations above the mean firing rate for that unit. Unsmoothed 2-D rate maps were used to determine the pixel adjacency criterion. Linearized spatial rate maps were utilized for all other analyses in the study. The linearized spatial rate maps were formed using 2.5 cm bins and were smoothed by convolution with a Gaussian kernel ($\sigma = 5$ cm).

Definition of Firing Field Edges

Firing fields were identified from the smoothed linearized spatial rate maps. A field must have three adjacent pixels (7.5 cm) that contained firing that exceeded 1Hz and two standard deviations above the mean firing rate for the unit. The width of each field was calculated as the number of pixels that were within 10% of the maximum firing rate of each field.

Pearson correlation

Pearson correlations were calculated according to the formula:

$$r = \frac{\sum_{i=1}^{n}(X_{i} - \overline{X})(Y_i - \overline{Y})}{\sqrt{\sum_{i=1}^{n}(X_{i} - \overline{X})^2} \sqrt{\sum_{i=1}^{n}(Y_{i} - \overline{Y})^2}}$$

where X_i is the firing rate of the i-th spatial bin of one period and Y_i is the i-th spatial bin during a different period. $\overline{X}$ and $\overline{Y}$ are the mean firing rates for the two conditions.

Spatial Information

The spatial information score, given in bits/spike, was calculated using the following equation:

$$I = \sum_{i=1}^{n} P_i \frac{Z_i}{\overline{Z}} \log_2 \frac{Z_i}{\overline{Z}}$$

where P_i is the probability of occupying the i-th spatial bin, Z_i is the firing rate in the i-th spatial bin and $\overline{Z}$ is the mean firing rate across all spatial bins (Skaggs et al., 1992).

Cosine Distance Analysis

Analyses of neural ensemble activity within each recording day were performed by collating linearized firing rate maps from the active place cells to form a population vector. Population vectors exclusively comprised neurons that met the place cell criteria, and a minimum of 10 place cells had to be active for a recording day to be considered for ensemble analysis. The cosine distance metric was utilized to quantify the similarity of the population vector from one epoch of interest to another (Komorowski et al., 2013). The distance between the population vectors from two epochs (x and y) was measured utilizing the cosine of the angle between the two vectors in N-dimensional space, where N is the number of neurons in the ensemble multiplied by the number of spatial bins in each neuron's rate map. The cosine distance between vectors x and y was calculated as follows:

$$cosine\ distance = 1 - \frac{x \cdot y}{\|x\|\|y\|}$$

The distance metric can range between 0 and 1, where 0 designates that the vectors are collinear and 1 designates that the vectors are orthogonal. Cosine distances that approach 0 indicate that the place cells composing the population vector have similar spatial firing

patterns between the two epochs, as defined by the relative firing rates across the spatial bins. Cosine distances that approach 1 indicate that each neuron inverted its spatial firing pattern, firing at high rates where they were once low and low rates where they were once high. Because these analyses were exclusively performed on ensembles of place cells, the sparseness of place cell firing patterns ensures that it is unlikely that the cosine distance between two population vectors will approach 1.

Statistical Analyses

The rate map correlations between periods of interest were calculated for each neuron. To characterize the non-normal distribution of changes in spatially specific firing across the population, the median correlations across conditions were compared with the Mann–Whitney U test (M–W) and the distributions of the correlations were compared with the Komolgorov-Smirnov test (KS). To visualize the distributions of correlations, cumulative density plots were created (Figure 3, Figure 5), where Pearson correlation is on the x-axis, and the y-value indicates what proportion of the population has a correlation that is less than or equal to each x-value. A distribution that falls on the left side of the plot has a large proportion of neurons with low correlation between the periods of interest. A one-way ANOVA was performed to compare the change between Baseline and Intervention ensemble vectors across conditions with Bonferroni corrected post-hoc tests for individual comparisons. A two-way, mixed-model, repeated-measures ANOVA was used to analyze the change in ensemble vectors as the Intervention period progressed.

Progressive changes during the Intervention period

The progressive changes that occurred over the course of the Intervention period are quantified in Figure 5 by comparing the linearized rate maps from the Baseline period to the rate maps from successive laps during the Intervention period. The changes in individual neurons were characterized by correlating the Baseline rate map to subsequent laps (Figure 5B–F). The changes in the ensemble coding during each day were quantified by collating the rate maps from the simultaneously recorded neurons, and determining the cosine distance between the aggregate Baseline rate map to the aggregate rate map of each subsequent lap (Figure 5G; see **Materials and Methods** for details about cosine distance analysis). To perform each of these analyses, a rate map was produced for the last 10 laps of the Baseline period. This epoch captures the spatial specificity of the neurons before the laser is turned on. Rate maps were then produced from a sliding window of 5 laps that were sampled in steps of 1 lap, which started during the Baseline and spanned to the end of the session. For the single-neuron correlations and the ensemble cosine distances, each rate map from the sliding window was compared against the rate map created from the last 10 laps of the Baseline period.

Histology

After completion of the behavioral experiments, rats were anesthetized with 2.5% isoflurane and small lesions were made at the end of the tetrodes by passing 40 µA of direct current through each wire. Animals were then injected with an overdose of pentobarbital sodium/ phenytoin sodium (Euthasol, Virbac Animal Health) and transcardially perfused with 0.05M

phosphate-buffered saline (PBS) followed by 4% paraformaldehyde in 0.05M PBS. The brain was removed and post-fixed in 4% paraformaldehyde for 2 hours and then cryoprotected using a 30% sucrose solution in 0.05M KPBS. Each brain was sliced into 30 μm sections in five series using a cryostat. One series was Nissl stained for anatomical confirmation of tetrode and fiber locations. Another series was immunohistochemically stained for GFP (1:50,000; Rabbit polyclonal anti-GFP for 48 hours, Novus Biologicals; 1:600; biotinylated Goat anti-Rabbit for 1 hour, Vector Labs). Sections were then processed with avidin-biotinylated horseradish peroxidase complex (Elite ABC Kit; Vector Labs), and reacted with nickel-diaminobenzidine (nickel (II) sulfate, 3,3'-Diaminobenzidine; Sigma) and H_2O_2 to visualize the extent of viral spread.

Results

A total of 2172 single cells were recorded from the dorsal CA1 region of 7 rats (4 ArchT and 3 GFP). Of these 2172 cells, a total of 1100 cells (50.64%) met criteria defining them as place cells (See **Materials and Methods** for place cell criteria) and were used in subsequent analysis. In rats expressing ArchT, we recorded 371 place cells on days (N = 28) in which the dorsocaudal region of the medial entorhinal cortex (MEC) underwent light-mediated inactivation (Laser; Figure 1E, top). As a within-animal control, ArchT rats also received Sham-Laser intervention days in which the laser was prevented from shining through the fiber optic (Sham-Laser; Figure 1E, bottom). For Sham-Laser intervention days (N = 20) in ArchT rats, we recorded a total of 288 place cells. In control rats expressing only GFP (and not ArchT) in the medial entorhinal cortex, a total of 237 place cells were recorded on Laser intervention days (N = 22), and 204 place cells on within-animal control, Sham-Laser intervention days (N = 16) (See **Materials and Methods** for details about the inactivation schedule).

MEC disruption alters CA1 spatial representations

Transient inactivation of activity in the MEC via ArchT resulted in a partial remapping of spatially selective activity within dorsal CA1 as animals traversed an elliptical track. To visualize the changes in spatial selectivity, separate spatial firing rate maps were constructed for the baseline (Baseline), the intervals in which rats received light-induced inactivation of MEC (Laser-On), and the intervals between laser stimulations (Laser-Off) (Figure 1E; See **Materials and Methods** for details about the inactivation schedule). Place cells exhibited multiple types of changes in activity (Figure 2). These changes could include the loss (Figure 2C) or gain (Figure 2D) of place field, or shifts in the preferred firing location of an existing field (Figure 2B). However, the remapping effect was not coherent across the population, as only a subset of neurons altered their firing patterns while others maintained stable firing fields (Figure 2A). Strikingly, most of the cells that exhibited place field changes between Baseline and Intervention periods maintained these differences during both Laser-On and Laser-Off intervals.

Place field changes were measured by first constructing linearized firing rate maps for all place cells during each experimental period. Place field changes were then quantified by calculating Pearson correlations between the firing rate maps constructed for each period. To

visualize how the correlations across the population differed between conditions, the data is combined from all rats and all days for each respective session type and graphed in cumulative density plots (Figure 3), where Pearson correlation is on the x-axis, and the y-value indicates what proportion of the population has a correlation that is less than or equal to each x-value. A distribution that falls on the left side of the plot has a large proportion of neurons with low correlation between the periods of interest.

Our initial characterization of the effects of MEC inactivation focused on comparing Laser-On periods to the Baseline. We observed that MEC inactivation induces significant remapping in the CA1 place cell population. In ArchT rats, spatial firing during Laser-On intervals was more dissimilar from the Baseline on Laser intervention days than Sham-Laser intervention days, as indicated by their correlation medians and distributions (Figure 3A; Median (Mdn) $_{\text{Laser(Baseline v Laser-On)}}$ = 0.7417, Mdn$_{\text{Sham-Laser(Baseline v Laser-On)}}$ = 0.8049, Mann-Whitney U test (M–W), U = −3.3074, p = 0.0009; Komolgorov-Smirnov test (K–S) = 0.1315, p = 0.0069). These results indicate that Laser intervention induced significant remapping in the pooled population of hippocampal neurons that surpassed random changes. Moreover, this difference between Laser intervention days and Sham-Laser intervention days was not observed in GFP rats (Figure 3B; Mdn$_{\text{Laser(Baseline v Laser-On)}}$ = 0.7678, Mdn$_{\text{Sham-Laser(Baseline v Laser-On)}}$ = 0.7778, M-W, U = −1.0476, p = 0.2948; K-S = 0.0726, p = 0.5991), demonstrating that the remapping observed in ArchT rats is not due to a non-specific effect of light stimulation. Together these results indicate that optogenetic inactivation of the MEC causes a significant change to the spatial representation in the hippocampus.

Transient, intermittent MEC disruption produces stable changes in CA1

If persistent input from the MEC is necessary for the moment-to-moment specificity of spatial representations in the hippocampus, then changes in CA1 activity would be time-locked to intervals of MEC disruption. Our ability to transiently disrupt MEC input allows us to directly test this hypothesis by examining whether CA1 neurons exhibit distinct activity profiles during laser (Laser-On) and between-laser (Laser-Off) intervals. However, we observed that the spatial mapping during Laser-On intervals was similar to Laser-Off intervals on Laser intervention days. The similarity between these intervals was not significantly different from Sham-Laser intervention days (Figure 3C; Mdn$_{\text{Laser(Laser-On v Laser-Off)}}$ = 0.9708, Mdn$_{\text{Sham-Laser(Laser-On v Laser-Off)}}$ = 0.9714, M-W, U = 0.4795, p = 0.6316; K-S = 0.0638, p = 0.5108), indicating that Laser inactivation did not affect the stability of the firing fields between the Laser-On and Laser-Off intervals. By contrasting the correlations of the Laser-On intervals and the Baseline (Figure 3A) with the correlations of Laser-On intervals with Laser-Off intervals (Figure 3C), it is evident that the spatial representations across the population strikingly change between the Baseline and Laser-On periods, but do not differ between Laser-On and Laser-Off. Together, these results indicate that the stark remapping from Baseline induced during the laser intervention period in ArchT rats persists across Laser-On and Laser-Off intervals.

All rats received a Recovery period 1–2 hours after the initial session to detect whether transient disruption of MEC input would affect subsequent re-engagement of the network.

Since the optogenetic manipulation of the MEC is reversible, it is possible that re-exposure to the elliptical track 1–2 hours after cessation of the manipulation would re-engage the original baseline network in the hippocampus. We instead observed that spatial representations during the Recovery period were more similar to the Laser-On period than to the Baseline (*not pictured*, $Mdn_{Laser(Baseline\ v\ Recovery)} = 0.5507$, $Mdn_{Laser(Laser-On\ v\ Recovery)} = 0.7670$, M-W, U-value = −7.1655, p < 0.00001). These results suggest that cessation of MEC disruption does not return the network to the initial baseline state. In addition, the similarity between Baseline and Recovery periods was comparable between Laser intervention days and Sham-Laser intervention days for ArchT rats ($Mdn_{Laser(Baseline\ v\ Recovery)} = 0.5507$, $Mdn_{Sham-Laser(Baseline\ v\ Recovery)} = 0.5467$, M-W, U = 1.2519, p = 0.2106) and GFP rats ($Mdn_{Laser(Baseline\ v\ Recovery)} = 0.2710$, $Mdn_{Sham-Laser(Baseline\ v\ Recovery)} = 0.4440$, M-W, U = −0.4203, p = 0.6743). There was also no significant difference between the correlations of Laser-On and Recovery periods on Laser intervention and Sham-Laser intervention days ($Mdn_{Laser(Laser-On\ v\ Recovery)} = 0.7670$, $Mdn_{Sham-Laser(Laser-On\ v\ Recovery)} = 0.7492$, M-W, U = 0.8832, p = 0.3771), indicating that the return of MEC activity during the Recovery period did not induce more changes in the network than were intrinsically generated on Sham-Laser days.

Summarily characterizing the extent of the remapping effect

In order to succinctly characterize the extent of remapping that was induced by MEC inactivation, the rate maps from the conclusion of the laser intervention period (10 laps) were compared to an equated Baseline period just before laser inactivation. Taking the last laps of the intervention period ensures that the full extent of the changes that gradually occur over the course of the intervention is appropriately captured. Given the high degree of similarity between Laser-On and Laser-Off intervals, these intervals were combined and considered as a single intervention period (Intervention). In concert with our prior analyses, laser inactivation in ArchT rats caused striking remapping across the pooled population of CA1 neurons by the end of the Intervention period. This was demonstrated by the significantly lower correlations between the Baseline and Intervention period on Laser intervention days than Sham-Laser intervention days (*not pictured*, $Mdn_{Laser(Baseline\ v\ Intervention)} = 0.8601$, $Mdn_{Sham-Laser(Baseline\ v\ Intervention)} = 0.9134$, M-W, U = 4.8179, p < 0.0001; K-S = 0.1829, *p* < 0.0001). No such difference was observed in GFP rats ($Mdn_{Laser(Baseline\ v\ Intervention)} = 0.9046$, $Mdn_{Sham-Laser(Baseline\ v\ Intervention)} = 0.9066$, M-W, U = 0.9997, p = 0.3175; K-S = 0.0989, *p* = 0.2237). These results corroborate that optogenetic inactivation of the MEC induces a marked change in the spatial mapping of the pooled CA1 neurons over the course of the Intervention period. Since this approach summarily captures the changes occurring during the Intervention period, we compared the end of the Baseline and the end of the Intervention periods for all subsequent analyses.

Remapping effect of intervention is consistent across recording days

It is possible that the set of single neurons recorded within the same session do not behave independently but rather as an ensemble representation of space. To explore whether the same remapping effects are observed at the level of simultaneously recorded neural ensembles, we quantified the similarity of ensemble firing patterns between the end of the Baseline and the end of the Intervention periods using the cosine value of the angle between

the population vectors from the two periods (See **Materials and Methods** for details about cosine distance analysis; Komorowski et al., 2013). Cosine distances can range between 0 and 1, with values that are near 0 indicating that the spatial tuning of the neurons was similar in the Baseline and Intervention period. The value of the cosine distances between the Baseline and Intervention periods was significantly different across groups (Figure 3D; ANOVA, $F(3,47) = 4.9984$; $p = 0.0043$). Post-hoc tests revealed that cosine distances were significantly greater on Laser days than Sham-Laser days in ArchT rats (Bonferroni post-hoc test, $T = 3.8301$, $p = 0.0023$) and the distribution of the cosine distances across days were significantly different (K-S = 0.6154, $p = 0.0063$). The greater cosine distances on Laser intervention days indicate that the CA1 ensembles are changing their spatial representations more on days when the MEC is inactivated. No differences were observed between Laser and Sham-Laser days in GFP rats (Figure 3D; Bonferroni post-hoc test, $T = 0.5436$, $p = 0.5893$; K-S = 0.2867, $p = 0.6319$). These results confirm that the MEC inactivation consistently resulted in remapping of the neural ensemble that significantly exceeded spontaneous change.

The integrity of spatial tuning remains intact

It is possible that the observed changes in spatial mapping were the result of an overall decrease in the ability of the hippocampus to represent space. To test this hypothesis, we examined whether laser intervention significantly altered the physiological properties of the neurons. To examine how the firing properties at the conclusion of the laser-inactivating period compared to an equated epoch just before laser inactivation, the last 10 laps of the Baseline were compared with the last 10 laps of the Intervention. The mean firing rates across the population during the Intervention period were not significantly different from the Baseline period in ArchT or GFP rats for either Laser or Sham-Laser days (Table 1: Mean Rate). There were also no significant differences in within-field maximum firing rates between Baseline and the Intervention (Table 1: Max Rate). These results suggest that the excitability of the place cell population was not disrupted by MEC inactivation. We then tested whether laser intervention altered the spatial firing properties of the neurons. There were no significant differences between Baseline and Intervention periods in spatial information content or the size of the fields across the population of neurons in ArchT or GFP rats for either Laser or Sham-Laser days (Table 1: Field Width, Spatial Information). This indicates that the hippocampal neurons maintained the ability to represent space with high fidelity as a population.

To further characterize potential physiological differences between Baseline and Intervention periods, we examined how firing properties changed within each neuron. For each firing property, we subtracted the value during the Baseline from the value at the end of the Intervention period for each neuron. The median change in mean firing rate, within-field maximum firing rate, and spatial information was close to zero, and there were no significant differences across groups or intervention types (Table 2). Together, these results indicate that changes during the Intervention period were evenly distributed across the population, yielding physiological characteristics similar to the Baseline period. Though any individual neuron may drastically change its firing properties, these findings suggest that

unilateral optogenetic inactivation of the MEC does not alter the ability of the network, as a whole, to represent space.

Despite a balance of changes across the hippocampal network, the extent of within-neuron changes in spatial information score was greater on Laser intervention days (Figure 4A). This is demonstrated by the distribution of the change in spatial information being significantly wider on Laser intervention days than the distribution observed on Sham-Laser intervention days in ArchT rats ($Mdn_{Laser(Baseline\ v\ Intervention)} = 0.0102$, $Mdn_{Sham-Laser(Baseline\ v\ Intervention)} = -0.0150$, M-W, $U = 0.1116$, $p = 0.9112$; one-tail K-S = 0.1079, $p = 0.0212$). Transient inactivation of MEC thus induced more changes in spatial information across the population without altering overall network excitability or the integrity of hippocampal spatial representations.

MEC disruption biases the active population of hippocampal neurons

To test whether distinct ensembles of neurons become active as a result of MEC inhibition, we identified populations of place cells that developed or lost spatial tuning between Baseline and Intervention periods. We then examined whether these changes occurred more often during MEC inactivation than during the other conditions. We found significant differences in the proportion of cells that either became active or inactive across groups (Figure 4B, χ^2 (3, N = 1100) = 48.1076, p < 0.00001), with the largest proportion of cells exhibiting this phenomenon in ArchT rats on Laser intervention days. We further determined that the proportion of neurons that gained a field was similar to the proportion of neurons that lost a field in ArchT rats on Laser intervention days, (Figure 4C, χ^2 (1, N = 371) = 0.2273, p = 0.6335). This result indicates that inactivating the MEC instigates a balanced shift in the population of active neurons, with a comparable number of neurons representing the environment in each period. Taken together, these findings suggest that the membership of neurons in the active ensemble is markedly altered as a result of the MEC disruption without compromising the integrity of the spatial representation.

The network impact of MEC disruption is cumulative

In order to quantify the progression of inactivation-induced remapping over time, we systematically evaluated the extent of place field changes during the course of the Intervention period with respect to Baseline. We observed that spatial representations across the population became progressively more dissimilar from the baseline over the course of the session (Figure 5A), as has been similarly observed in previous studies (Mankin et al., 2012; Manns et al., 2007). Correlations were assessed between the last 10 laps of the Baseline period and a sliding window of 5 laps during the Intervention period that advanced in steps of 10 laps. Progressive changes occurred in ArchT rats for both Laser intervention days (Figure 5B, Friedman test$_{(Laser)}$, $\chi^2 = 22.1$, d.f. = 2, p < 0.0001) and Sham-Laser intervention days (Figure 5C, Friedman test$_{(Sham-Laser)}$, $\chi^2 = 8.98$, d.f. = 2, p = 0.0112). Importantly, we found that MEC inactivation significantly increased the degree of change across the population as laps progressed when compared to Sham-Laser intervention days (Figure 5D–F, $Mdn_{Laser(Baseline\ v\ 6–10)} = 0.8966$, $Mdn_{Sham-Laser(Baseline\ v\ 6–10)} = 0.9200$, M-W, $U = 3.2434$, $p = 0.0012$; $Mdn_{Laser(Baseline\ v\ 16–20)} = 0.8850$, $Mdn_{Sham-Laser(Baseline\ v\ 16–20)} = 0.9194$, M-W, $U = 3.2316$, $p = 0.0012$;

$Mdn_{Laser(Baseline\ v\ 26-30)} = 0.8568$, $Mdn_{Sham-Laser(Baseline\ v\ 26-30)} = 0.9009$, M-W, U = 3.1589, p = 0.0016). We observed that the degree of change after the first 10 laps on Laser intervention days could only be seen after 30 laps on Sham-Laser intervention days. To quantify this difference, we contrasted the change that occurred after the first 10 laps on Laser intervention days to the changes observed every 10 laps on Sham-Laser intervention days (Figure 5D,E, $Mdn_{Laser(Baseline\ v\ 6-10)} = 0.8966$, $Mdn_{Sham-Laser(Baseline\ v\ 16-20)} = 0.9194$, M-W, U = 2.1852, p = 0.0289; $Mdn_{Laser(Baseline\ v\ 6-10)} = 0.8966$, $Mdn_{Sham-Laser(Baseline\ v\ 26-30)} = 0.9009$, M-W, U = 0.8268, p = 0.4083). The pronounced changes that occurred within the initial laps of the Intervention period suggest that place field remapping began soon after the MEC inactivation.

The progressive changes also manifested in the ensemble analyses of individual days. To quantify the magnitude of change that occurred as the Intervention period progressed, the cosine distance between the population vectors from the Baseline and a sliding window of 5 laps during the Intervention period was calculated for the simultaneously recorded CA1 ensembles (Figure 5G). A mixed-model, 2-way repeated-measures ANOVA was performed to assess the progression of changes on successive laps during Laser and Sham-Laser intervention days (*intervention* X *laps after baseline*). In accordance with the our findings demonstrating increased remapping with MEC inactivation, there was a significant main effect between Laser and Sham-Laser interventions (F(1,725) = 20.5034, p = 0.0001). The analysis also demonstrated that MEC inactivation increased the progression of change over the course of the Intervention period, as indicated by the significant interaction effect between the type of intervention and the number of laps after baseline (F(29,725) = 4.0221, p < 0.0001).

Discussion

Our study provides further evidence that spatial representations in the hippocampus are governed by at least two dissociable mechanisms: determining which neurons will be active in a given environment and creating spatially selective responses in the active neurons. Our results indicate that transient, partial inactivations of the MEC can alter the active population of hippocampal neurons in an environment, while the integrity of the spatial representations among neurons in the newly active ensemble is maintained. The time course of the observed changes did not follow the acute timing of the MEC inactivation, indicating that while MEC disruption biases which cell assembly is likely to be active, there are additional mechanisms driving and stabilizing the population of active hippocampal neurons.

The partial optogenetic inactivation of the MEC changed spatial representations in the hippocampus such that distinct patterns of active neurons were seen between baseline and laser conditions (Figure 2). These distinct patterns reflected remapping of spatially selective activity, including the selective recruitment of new fields and the silencing of previously active neurons (Figure 2C,D; Figure 4C,D; Figure 5A). The correlations of spatial firing maps between baseline and inactivation periods across the population were significantly lower than Sham-Laser Intervention days (Figure 3A). Importantly, we observed that changes in spatial information were balanced across the network, indicating that the integrity of the hippocampal spatial representations was similar across each period (Table 1; Table 2;

Figure 4A). This suggests that inconsistent MEC input does not broadly decrease the integrity of spatial tuning across the population, but instead influences which ensemble representation will be active in the hippocampal network. A previous study has demonstrated the converse of this dichotomy by showing that interfering with the intrinsic communication of the hippocampus diminishes spatial tuning in place cells, but the reliable selection of the impoverished spatial map for a particular environment remains intact (Cacucci et al., 2007). Together these findings suggest that there is a dissociation between these mechanisms, and that the MEC may have a critical role in biasing the population of spatially selective neurons that represent the environment.

Notably, shifts in the active population of neurons within the hippocampus remained stable during the Intervention period despite phasic disruption of MEC input. This could be seen in the high correlations between activity during the Laser-On and Laser-Off intervals (Figure 3C). These results suggest that once CA1 neurons undergo a change, they are robust to interference from inconsistent MEC input. We propose that the repeated, intermittent disruption of MEC output critically destabilizes the network of hippocampal neurons representing the environment. The hippocampal network then remaps and stabilizes utilizing the remaining inputs that have a more consistent impact over time. Consequently, when input from the inactivated region of MEC returns, it has a diminished effect relative to the inputs that remained extant throughout the inactivation period (Figure 6). This hypothesis is further supported by the observed similarity of hippocampal representations between Intervention and Recovery periods despite the restoration of MEC activity. This suggests that there is a sustained network modification that maintains the active cell assembly irrespective of the availability of input from the inconsistent MEC neurons.

Attractor dynamics within the hippocampal network have been proposed to mediate the ability of the hippocampus to stabilize the appropriate map from an impoverished input (Hasselmo et al., 1995; McNaughton et al., 2006; Rolls, 2007; Treves and Rolls, 1992; Tsodyks, 2005). It is hypothesized that the elaborate recurrent connectivity of CA3 facilitates the continuous recruitment of members within a cell assembly, though other regions of the medial temporal lobe may contribute. Using a continuous attractor framework, populations of place cells sequentially fire as the rat progresses around the track, potentiating the neurons within the same cell assembly through recurrent excitation while suppressing competing maps through lateral inhibition (Colgin et al., 2010; Itskov et al., 2011; Knierim and Zhang, 2012; McNaughton et al., 2006; Samsonovich and McNaughton, 1997). This continual competition between cell assemblies serves to sustain and stabilize the spatial representation carried by the active population.

With our inactivation of MEC, we intermittently alter the input to the network, which could repeatedly disrupt the competitive balance of the continuous attractors in the hippocampus. In accordance with this theory, we observed an enhanced level of remapping that gradually occurred over the course of the Intervention period (Figure 5). A previous study has observed a similar gradual remapping in intact animals as they were exposed to serial presentations of mazes with graded differences in their shape (Leutgeb et al., 2005). This suggests that our partial inactivation of the MEC has an effect on the hippocampal network that is similar to making subtle gradual changes to environmental cues. Through periodic

disruption of inputs that support the balance of the competitive cell populations, we provide insight into the mechanism through which the membership of the cell assembly can be modified.

This gradual shift in the active population of hippocampal neurons can be contrasted against coherent changes that occur simultaneously across the entire hippocampal network. Previous studies have shown that distinct spatial representations within the hippocampus are not simultaneously active (Jezek et al., 2011; Kelemen and Fenton, 2010; Skaggs and McNaughton, 1998; Wills et al., 2005). The recruitment of orthogonal, functionally distinct ensembles enables the selection of discrete representations according to the most relevant spatial map. We did not observe these stark coherent changes across the whole cell assembly with our partial inactivation. Our findings suggest that broad coordination across extrinsic afferents may be necessary for switches between wholly orthogonal representations. We propose that sustained coordination of reliable afferents biases the attractor dynamics of the hippocampus, while the bias from inconsistent inputs is progressively marginalized as the attractor stabilizes.

The mechanisms that give rise to the flexible selection of distinct maps may serve as the basis for context-guided memory retrieval. The recognition of a set of circumstances may instigate coordinated activity across a wide swath of hippocampal afferents, which in turn allows for orthogonal representations to become active for each discrete circumstance. Our partial inactivation of the MEC produced distinct but not orthogonal maps, and provided insight into the extent of coordination across afferents that would be required to produce fully discrete representations. We find that the MEC has a critical role in biasing the participation of neurons in the network, and therefore mediates the ability of the hippocampus to selectively represent information.

Acknowledgements

References

Alme CB, Miao C, Jezek K, Treves A, Moser EI, Moser M-B. Place cells in the hippocampus: Eleven maps for eleven rooms. Proc. Natl. Acad. Sci. 2014; 111:201421056.

Bjerknes TL, Moser EI, Moser M-B. Representation of geometric borders in the developing rat. Neuron. 2014; 82:71–78. [PubMed: 24613417]

Boyden ES. A history of optogenetics: the development of tools for controlling brain circuits with light. F1000 Biol. Rep. 2011; 3:11. [PubMed: 21876722]

Brandon MP, Koenig J, Leutgeb JK, Leutgeb S. New and distinct hippocampal place codes are generated in a new environment during septal inactivation. Neuron. 2014; 82:789–796. [PubMed: 24853939]

Cacucci F, Wills TJ, Lever C, Giese KP, O'Keefe J. Experience-dependent increase in CA1 place cell spatial information, but not spatial reproducibility, is dependent on the autophosphorylation of the alpha-isoform of the calcium/calmodulin-dependent protein kinase II. J. Neurosci. 2007; 27:7854–7859. [PubMed: 17634379]

Van Cauter T, Poucet B, Save E. Unstable CA1 place cell representation in rats with entorhinal cortex lesions. Eur. J. Neurosci. 2008; 27:1933–1946. [PubMed: 18412614]

Colgin LL, Leutgeb S, Jezek K, Leutgeb JK, Moser EI, McNaughton BL, Moser M-B. Attractor-map versus autoassociation based attractor dynamics in the hippocampal network. J. Neurophysiol. 2010; 104:35–50. [PubMed: 20445029]

Dupret D, O'Neill J, Pleydell-Bouverie B, Csicsvari J. The reorganization and reactivation of hippocampal maps predict spatial memory performance. Nat. Neurosci. 2010; 13:995–1002. [PubMed: 20639874]

Eichenbaum H, Sauvage M, Fortin N, Komorowski R, Lipton P. Towards a functional organization of episodic memory in the medial temporal lobe. Neurosci. Biobehav. Rev. 2012; 36:1597–1608. [PubMed: 21810443]

Fyhn M, Molden S, Witter MP, Moser EI, Moser M-B. Spatial representation in the entorhinal cortex. Science. 2004; 305:1258–1264. [PubMed: 15333832]

Fyhn M, Hafting T, Treves A, Moser M-B, Moser EI. Hippocampal remapping and grid realignment in entorhinal cortex. Nature. 2007; 446:190–194. [PubMed: 17322902]

Giocomo LM, Stensola T, Bonnevie T, Van Cauter T, Moser M-B, Moser EI. Topography of head direction cells in medial entorhinal cortex. Curr. Biol. 2014; 24:252–262. [PubMed: 24440398]

Hafting T, Fyhn M, Molden S, Moser M-B, Moser EI. Microstructure of a spatial map in the entorhinal cortex. Nature. 2005; 436:801–806. [PubMed: 15965463]

Hales JB, Schlesiger MI, Leutgeb JK, Squire LR, Leutgeb S, Clark RE. Medial entorhinal cortex lesions only partially disrupt hippocampal place cells and hippocampus-dependent place memory. Cell Rep. 2014; 9:893–901. [PubMed: 25437546]

Han X, Chow BY, Zhou H, Klapoetke NC, Chuong A, Rajimehr R, Yang A, Baratta MV, Winkle J, Desimone R, et al. A high-light sensitivity optical neural silencer: development and application to optogenetic control of non-human primate cortex. Front. Syst. Neurosci. 2011; 5:18. [PubMed: 21811444]

Hasselmo ME, Schnell E, Barkai E. Dynamics of learning and recall at excitatory recurrent synapses and cholinergic modulation in rat hippocampal region CA3. J. Neurosci. 1995; 15:5249–5262. [PubMed: 7623149]

Itskov V, Curto C, Pastalkova E, Buzsáki G. Cell assembly sequences arising from spike threshold adaptation keep track of time in the hippocampus. J. Neurosci. 2011; 31:2828–2834. [PubMed: 21414904]

Jezek K, Henriksen EJ, Treves A, Moser EI, Moser M-B. Theta-paced flickering between place-cell maps in the hippocampus. Nature. 2011; 478:246–249. [PubMed: 21964339]

Kelemen E, Fenton AA. Dynamic grouping of hippocampal neural activity during cognitive control of two spatial frames. PLoS Biol. 2010; 8:e1000403. [PubMed: 20585373]

Knierim JJ, Zhang K. Attractor dynamics of spatially correlated neural activity in the limbic system. Annu. Rev. Neurosci. 2012; 35:267–285. [PubMed: 22462545]

Komorowski RW, Manns JR, Eichenbaum H. Robust conjunctive item-place coding by hippocampal neurons parallels learning what happens where. J. Neurosci. 2009; 29:9918–9929. [PubMed: 19657042]

Komorowski RW, Garcia CG, Wilson A, Hattori S, Howard MW, Eichenbaum H. Ventral hippocampal neurons are shaped by experience to represent behaviorally relevant contexts. J. Neurosci. 2013; 33:8079–8087. [PubMed: 23637197]

Leutgeb JK, Leutgeb S, Treves A, Meyer R, Barnes CA, McNaughton BL, Moser MB, Moser EI. Progressive transformation of hippocampal neuronal representations in "morphed" environments. Neuron. 2005; 48:345–358. [PubMed: 16242413]

Mankin EA, Sparks FT, Slayyeh B, Sutherland RJ, Leutgeb S, Leutgeb JK. Neuronal code for extended time in the hippocampus. Proc. Natl. Acad. Sci. U. S. A. 2012; 109:19462–19467. [PubMed: 23132944]

Manns JR, Howard MW, Eichenbaum H. Gradual changes in hippocampal activity support remembering the order of events. Neuron. 2007; 56:530–540. [PubMed: 17988635]

Markus EJ, Qin YL, Leonard B, Skaggs WE, McNaughton BL, Barnes CA. Interactions between location and task affect the spatial and directional firing of hippocampal neurons. J. Neurosci. 1995; 15:7079–7094. [PubMed: 7472463]

McNaughton BL, Battaglia FP, Jensen O, Moser EI, Moser M-B. Path integration and the neural basis of the "cognitive map". Nat. Rev. Neurosci. 2006; 7:663–678. [PubMed: 16858394]

Miller VM, Best PJ. Spatial correlates of hippocampal unit activity are altered by lesions of the fornix and endorhinal cortex. Brain Res. 1980; 194:311–323. [PubMed: 7388617]

Moita MAP, Rosis S, Zhou Y, LeDoux JE, Blair HT. Putting fear in its place: remapping of hippocampal place cells during fear conditioning. J. Neurosci. 2004; 24:7015–7023. [PubMed: 15295037]

Muller RU, Kubie JL. The effects of changes in the environment on the spatial firing of hippocampal complex-spike cells. J. Neurosci. 1987; 7:1951–1968. [PubMed: 3612226]

Navawongse R, Eichenbaum H. Distinct pathways for rule-based retrieval and spatial mapping of memory representations in hippocampal neurons. J. Neurosci. 2013; 33:1002–1013. [PubMed: 23325238]

O'Keefe J, Dostrovsky J. The hippocampus as a spatial map. Preliminary evidence from unit activity in the freely-moving rat. Brain Res. 1971; 34:171–175. [PubMed: 5124915]

O'Keefe, J.; Nadel, L. The hippocampus as a cognitive map. Oxford: University Press; 1978.

Rolls ET. An attractor network in the hippocampus: theory and neurophysiology. Learn Mem. 2007; 14:714–731. [PubMed: 18007016]

Rolls ET, Stringer SM, Elliot T. Entorhinal cortex grid cells can map to hippocampal place cells by competitive learning. Network. 2006; 17:447–465. [PubMed: 17162463]

Samsonovich A, McNaughton BL. Path integration and cognitive mapping in a continuous attractor neural network model. J. Neurosci. 1997; 17:5900–5920. [PubMed: 9221787]

Sargolini F, Fyhn M, Hafting T, McNaughton BL, Witter MP, Moser M-B, Moser EI. Conjunctive representation of position, direction, and velocity in entorhinal cortex. Science. 2006; 312:758–762. [PubMed: 16675704]

Savelli F, Knierim JJ. Hebbian analysis of the transformation of medial entorhinal grid-cell inputs to hippocampal place fields. J. Neurophysiol. 2010; 103:3167–3183. [PubMed: 20357069]

Schlesiger MI, Cannova CC, Boublil BL, Hales JB, Mankin EA, Brandon MP, Leutgeb JK, Leibold C, Leutgeb S. The medial entorhinal cortex is necessary for temporal organization of hippocampal neuronal activity. Nat. Neurosci. 2015; 18:1123–1132. [PubMed: 26120964]

Skaggs WE, McNaughton BL. Spatial firing properties of hippocampal CA1 populations in an environment containing two visually identical regions. J. Neurosci. 1998; 18:8455–8466. [PubMed: 9763488]

Skaggs WE, McNaughton BL, Gothard KM. An Information-Theoretic Approach to Deciphering the Hippocampal Code. 1992:1030–1037.

Treves A, Rolls ET. Computational constraints suggest the need for two distinct input systems to the hippocampal CA3 network. Hippocampus. 1992; 2:189–199. [PubMed: 1308182]

Tsodyks M. Attractor neural networks and spatial maps in hippocampus. Neuron. 2005; 48:168–169. [PubMed: 16242397]

Wills TJ, Lever C, Cacucci F, Burgess N, O'Keefe J. Attractor dynamics in the hippocampal representation of the local environment. Science. 2005; 308:873–876. [PubMed: 15879220]
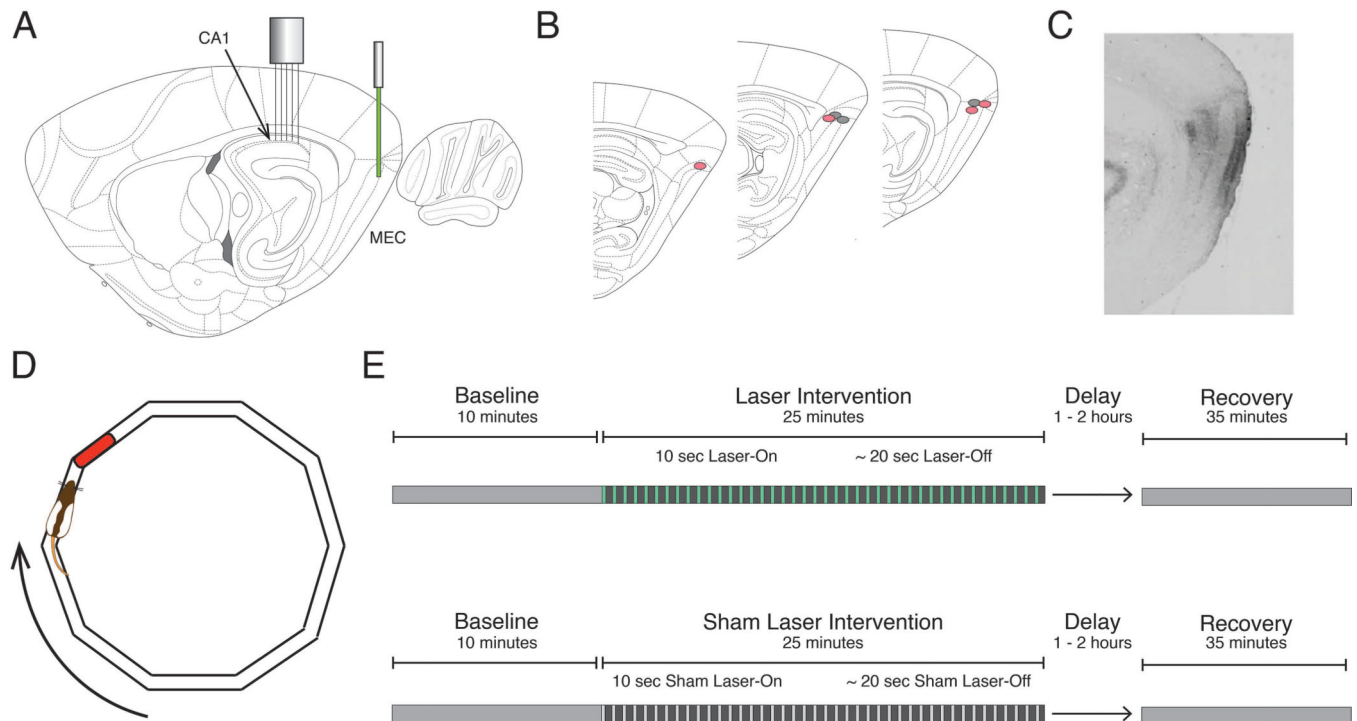
**Figure 1. Schematic of the inactivation procedure and task design**

A, Optogenetic inactivation of the dorsocaudal medial entorhinal cortex (MEC) was achieved using a 532 nm laser to activate the inhibitory opsin ArchT. Simultaneous electrophysiological recordings were performed in the ipsilateral dorsal CA1. **B**, Reconstruction of optic fiber tip locations. Red and gray circles correspond to rats expressing ArchT or GFP, respectively. **C**, Representative sagittal section from a rat expressing ArchT, indicating the spread of viral infection in the MEC. **D**, For every phase of the experiment, rats completed laps on an elliptical track for a food reward in a reliably rewarded location (*red*). **E**, Experimental paradigms for both Laser (*top*) and Sham Laser (*bottom*) intervention days consisted of a Baseline period, an Intervention period (constituted by 30 alternating 10-second Laser-On and ~20-second Laser-Off intervals), and a Recovery period.
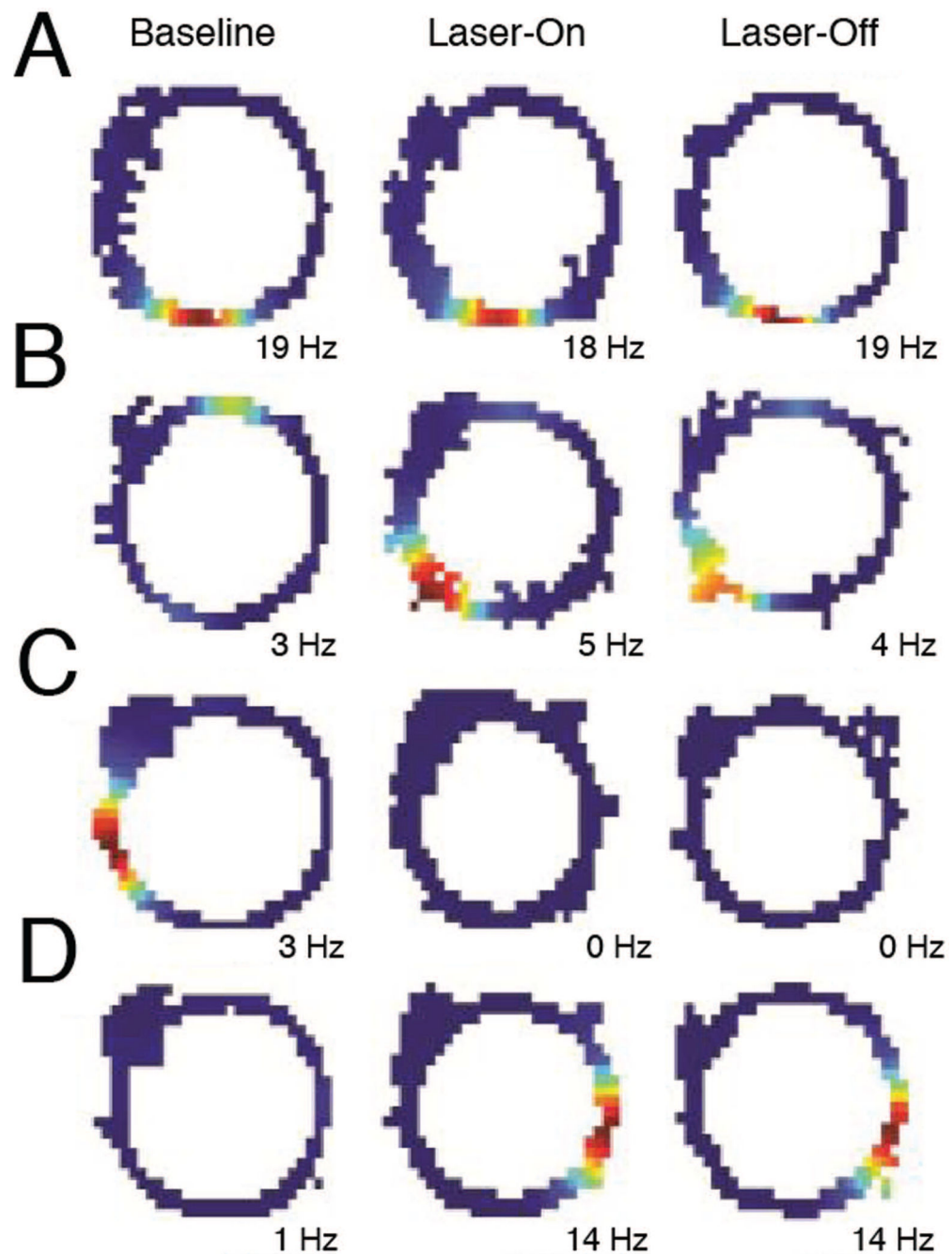
Figure 2. MEC inactivation affects spatial firing in CA1

Representative firing rate maps indicating the place cell activity on the elliptical track during baseline (left), Laser-On (middle), and Laser-Off (right) periods. Warm colors indicate higher firing rates, with the maximum firing rate indicated at the bottom of each map. CA1 neurons exhibited many different responses during the intervention period, including: *A*, stable place fields, *B*, a shifted place fields, *C*, loss of fields, and *D*, gain of fields. Most of the cells that exhibited place field changes between baseline and intervention periods maintained these differences during both Laser-On and Laser-Off intervals.
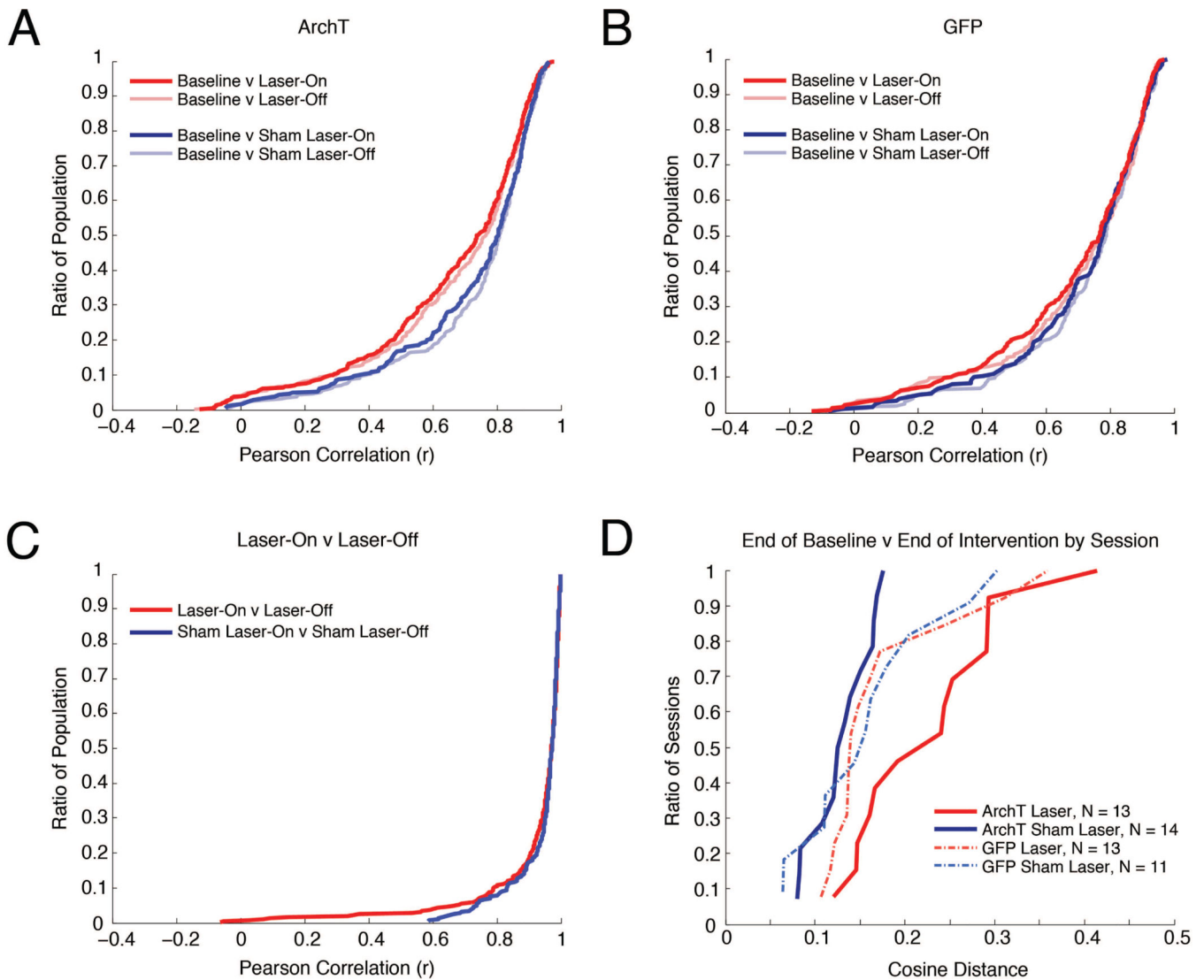
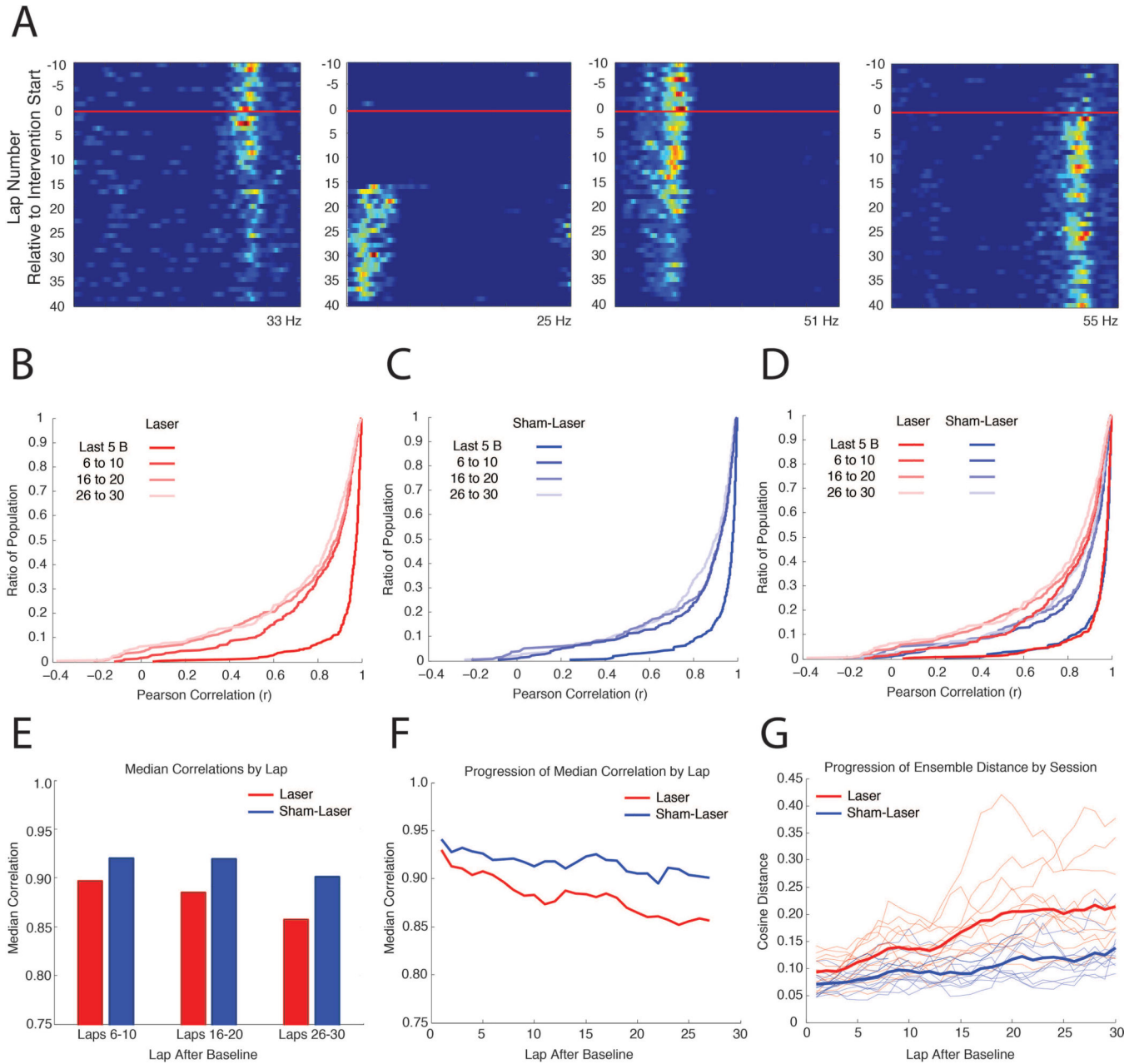**Figure 3. Transient MEC inactivation produces stable changes in CA1**
A, Cumulative density plots where the y-value indicates the ratio of the population that has a correlation less than or equal to each x-value, illustrating comparisons of spatial activity across baseline, Laser-On, and Laser-Off intervals in ArchT rats on Laser and Sham Laser intervention days. **B**, Same as in (**A**), for GFP rats. **C**, Cumulative density plots illustrating Laser-On v Laser-Off comparisons on Laser and Sham Laser intervention days in ArchT rats. **D**, Comparison of the neural ensemble representation of space between last 10 laps of the Baseline and last 10 laps of the Intervention period for each recording day. For each experimental condition, the distribution of cosine distances between the neural ensemble vectors during the Baseline and Intervention periods is charted in a cumulative density plot.
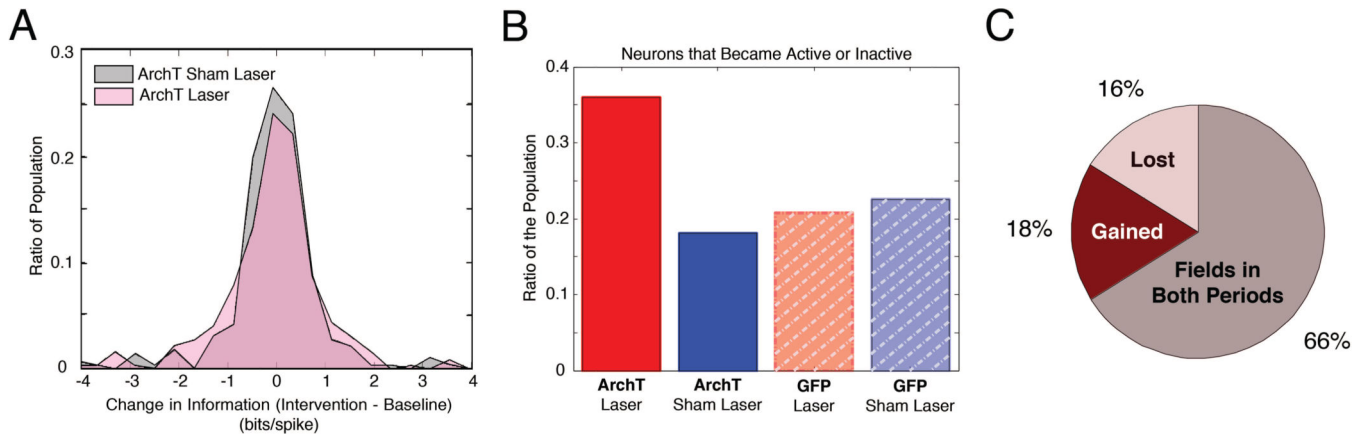
**Figure 4. MEC inactivation biases the active population of hippocampal cells**

A, The distribution of changes in spatial information on Laser intervention days (*pink*) and Sham Laser intervention days (*gray*). Changes in spatial information were balanced, with a greater proportion of cells exhibiting large changes on laser intervention days. *B*, The proportion of cells that became active or inactive during the intervention period in ArchT or GFP rats on Laser intervention or Sham Laser intervention days. These changes occurred more often in ArchT rats on laser intervention days. *C*, The proportions of cells that gained (*red*) or lost (*pink*) a place field in ArchT rats on laser intervention days were not significantly different.

Figure 5. The network impact of MEC disruption is cumulative

A, Representative linearized rate maps for four CA1 cells from ArchT rats during a Laser intervention day, demonstrating the heterogeneous time course of changes during the Intervention period. The x-axis indicates the spatial position of the elliptical track and the y-axis indicates the lap number with respect to the start of the intervention period (*red line*). Warm colors indicate higher firing rates, with the maximum firing rate displayed at the bottom of each map. *B*, Cumulative distribution plots where the y-value indicates the ratio of the population that has a correlation less than or equal to each x-value, illustrating comparisons between the last 10 laps during the Baseline and 5 lap blocks during the Intervention period for ArchT rats, advancing in steps of 10 laps. *C*, Same as in (*B*), on

Sham-Laser intervention days. **D**, Combined plots from (**B**) and (**C**) for visual comparison. **E**, Median values of the correlations in (**C**). **F**, Median values of the correlations between the last 10 laps during the Baseline and a 5 lap sliding window during the Intervention period, advancing in steps of 1 lap. **G**, Progressive change in ensemble similarity over the course of the Intervention for ArchT rats. The cosine distance between the population vector from the last 10 laps during the Baseline and a 5 lap sliding window during the Intervention period, advancing in steps of 1 lap, is plotted for each day (thin lines). Only days with 10 or more place cells were included. Thick lines represent the averaged cosine distance of each lap for the Laser and Sham-Laser days.
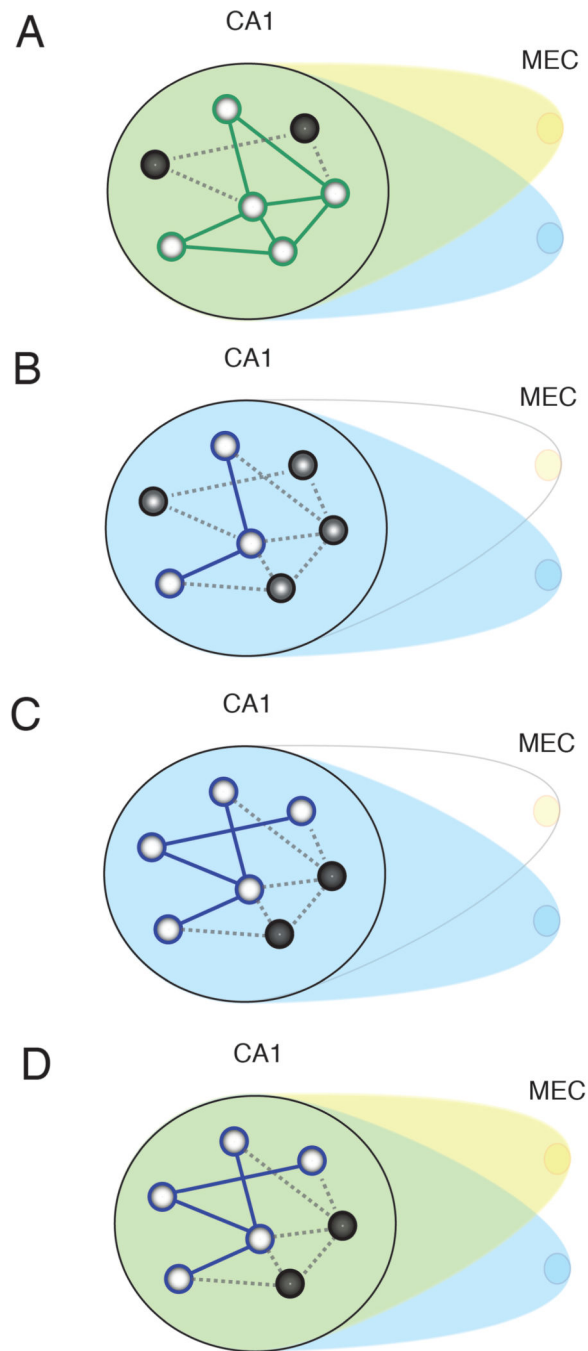
Figure 6. Summary diagram illustrating the effects of transient MEC disruption
A, CA1 initially receives input from distributed MEC afferents (*yellow* and *blue*). Light circles in CA1 indicate cells activated by the current inputs, and dark circles indicate inactive cells. Green lines represent the active attractor network, influenced by both blue and yellow afferents. Dotted lines represent inactive portions of the network. *B*, Transient inactivation of a circumscribed region of MEC destabilizes the existing attractor. *C*, A new attractor (*blue lines*) is stabilized by remaining inputs as the inconsistent inputs are

marginalized over time. **D**, When previously disrupted MEC input returns, it no longer has a strong influence on the CA1 network, and the new attractor in (**C**) persists.

Table 1

Spatial firing properties of CA1 neurons remain intact

There were no significant differences in mean firing rate, max firing rate, field width, or spatial information as a result of MEC disruption. Median values and distributions of medians were tested for significant differences between the Baseline and Intervention periods (Laser or Sham-Laser) in ArchT and GFP rats.

| Comparison | Mean Rate | | | | Max Rate | | | |
| | Mann-Whitney U | | K-S | | Mann-Whitney U | | K-S | |
	p-value	U-value	p-value	K-S stat	p-value	U-value	p-value	K-S stat
ArchT Baseline v Laser	0.8393	0.2028	0.7652	0.0485	0.5677	0.5714	0.8223	0.0458
ArchT Baseline v Sham-Laser	0.7378	0.3347	0.8777	0.0486	0.8686	0.1655	0.8777	0.0486
GFP Baseline v Laser	0.2927	1.0522	0.2032	0.0970	0.7890	0.2676	0.9563	0.0464
GFP Baseline v Sham-Laser	0.9565	0.0546	0.9971	0.0392	0.8858	0.1436	0.9630	0.0490

Mean Rate — Medians (Hz):
ArchT $_{\text{Laser (Baseline)}}$ = 1.24
ArchT $_{\text{Sham-Laser (Baseline)}}$ = 1.30
ArchT $_{\text{Laser (Intervention)}}$ = 1.19
ArchT $_{\text{Sham-Laser (Intervention)}}$ = 1.29
GFP $_{\text{Laser (Baseline)}}$ = 1.19
GFP $_{\text{Sham-Laser (Baseline)}}$ = 1.16
GFP $_{\text{Laser (Intervention)}}$ = 1.40
GFP $_{\text{Sham-Laser (Intervention)}}$ = 1.19

Max Rate — Medians (Hz):
ArchT $_{\text{Laser (Baseline)}}$ = 11.29
ArchT $_{\text{Sham-Laser (Baseline)}}$ = 12.14
ArchT $_{\text{Laser (Intervention)}}$ = 10.86
ArchT $_{\text{Sham-Laser (Intervention)}}$ = 11.50
GFP $_{\text{Laser (Baseline)}}$ = 11.49
GFP $_{\text{Sham-Laser (Baseline)}}$ = 11.61
GFP $_{\text{Laser (Intervention)}}$ = 11.93
GFP $_{\text{Sham-Laser (Intervention)}}$ = 11.04

| Comparison | Field Width | | | | Information | | | |
| | Mann-Whitney U | | K-S | | Mann-Whitney U | | K-S | |
	p-value	U-value	p-value	K-S stat	p-value	U-value	p-value	K-S stat
ArchT Baseline v Laser	0.1712	1.3682	0.1597	0.0890	0.6698	0.4265	0.9506	0.0377
ArchT Baseline v Sham-Laser	0.5343	0.6214	0.6853	0.0590	0.8780	0.1535	0.6845	0.0590
GFP Baseline v Laser	0.0725	1.7959	0.3221	0.0877	0.2140	1.2427	0.4858	0.0759
GFP Baseline v Sham-Laser	0.5215	0.6411	0.9723	0.0489	0.6003	0.5239	0.4615	0.0833

Field Width — Medians (2.5 cm bins):
ArchT $_{\text{Laser (Baseline)}}$ = 21
ArchT $_{\text{Sham-Laser (Baseline)}}$ = 20
ArchT $_{\text{Laser (Intervention)}}$ = 22
ArchT $_{\text{Sham-Laser (Intervention)}}$ = 20
GFP $_{\text{Laser (Baseline)}}$ = 19
GFP $_{\text{Sham-Laser (Baseline)}}$ = 19.5
GFP $_{\text{Laser (Intervention)}}$ = 20
GFP $_{\text{Sham-Laser (Intervention)}}$ = 20

Information — Medians (bits/spike):
ArchT $_{\text{Laser (Baseline)}}$ = 2.07
ArchT $_{\text{Sham-Laser (Baseline)}}$ = 2.06
ArchT $_{\text{Laser (Intervention)}}$ = 2.01
ArchT $_{\text{Sham-Laser (Intervention)}}$ = 2.05
GFP $_{\text{Laser (Baseline)}}$ = 2.08
GFP $_{\text{Sham-Laser (Baseline)}}$ = 2.15
GFP $_{\text{Laser (Intervention)}}$ = 2.06
GFP $_{\text{Sham-Laser (Intervention)}}$ = 2.09

Table 2

Changes in the spatial firing properties of CA1 neurons were even across groups, with a greater degree of spatial information changes in ArchT rats on laser intervention days

The median changes in mean firing rate, max firing rate, and spatial information (Δ = Intervention - Baseline) were not significantly different across Laser intervention and Sham-Laser intervention days or across ArchT or GFP treatment groups. The distribution of changes in spatial information was significantly different between ArchT$_{Laser}$ and ArchT$_{Sham-Laser}$ days and between ArchT$_{Laser}$ and GFP$_{Laser}$ groups.

Comparison	Mean Rate				Max Rate				Information			
	Mann-Whitney U		K-S		Mann-Whitney U		K-S		Mann-Whitney U		K-S	
	p-value	U-value	p-value	K-S stat	p-value	U-value	p-value	K-S stat	p-value	U-value	p-value	K-S stat
ArchT$_{Laser}$ **ArchT**$_{Sham-Laser}$	0.9393	0.0761	0.9393	0.0761	0.5469	0.6025	0.0761	0.0994	0.9112	0.1116	0.0423	0.1079
ArchT$_{Laser}$ **GFP**$_{Laser}$	0.1215	1.5484	0.1215	1.5484	0.4984	0.6770	0.4915	0.0685	0.0878	1.7071	0.0561	0.1100
ArchT$_{Laser}$ **GFP**$_{Sham-Laser}$	0.8327	0.2111	0.8327	0.2111	0.9166	0.1047	0.4618	0.0735	0.6389	0.4693	0.1714	0.0955
ArchT$_{Sham-Laser}$ **GFP**$_{Laser}$	0.1384	1.4814	0.1384	1.4814	0.8794	0.1518	0.9244	0.0476	0.0529	1.9359	0.0701	0.1123
ArchT$_{Sham-Laser}$ **GFP**$_{Sham-Laser}$	0.7891	0.2674	0.7891	0.2674	0.5600	0.5828	0.7843	0.0592	0.5514	0.5957	0.7843	0.0592
GFP$_{Laser}$ **GFP**$_{Sham-Laser}$	0.2830	1.0734	0.2830	1.0734	0.4936	0.6845	0.7180	0.0656	0.2031	1.2728	0.1366	0.1093
Median Values:	**ArchT**$_{Laser}$ = −0.03 Hz **ArchT**$_{Sham-Laser}$ = −0.09 **GFP**$_{Laser}$ = −0.02 **GFP**$_{Sham-Laser}$ = −0.08				**ArchT**$_{Laser}$ = −0.29 Hz **ArchT**$_{Sham-Laser}$ = −0.57 **GFP**$_{Laser}$ = −0.34 **GFP**$_{Sham-Laser}$ = −0.67				**ArchT**$_{Laser}$ = 0.01 bits/spike **ArchT**$_{Sham-Laser}$ = −0.02 **GFP**$_{Laser}$ = −0.16 **GFP**$_{Sham-Laser}$ = −0.05			